Wind and Structures, Vol. 13, No. 4 (2010) 327-346
DOI: http://dx.doi.org/10.12989/was.2010.13.4.327

Dynamic characteristics of transmission line conductors and behaviour under turbulent downburst loading

Mohamed M. Darwish[1], *Ashraf A. El Damatty[1] and Horia Hangan[2]

[1]Department of Civil and Environmental Engineering,
The University of Western Ontario London, Ontario, Canada, N6A 5B9
[2]Boundary Layer Wind Tunnel, The University of Western Ontario London, Ontario, Canada, N6A 5B9
(Received November 13, 2009, Accepted February 20, 2010)

Abstract. During the past decade, many electrical transmission tower structures have failed during downburst events. This study is a part of a research program aimed to understand the behaviour of transmission lines under such localized wind events. The present study focuses on the assessment of the dynamic behaviour of the line conductors under downburst loading. A non-linear numerical model, accounting for large deformations and the effect of pretension loading, is developed and used to predict the natural frequencies and mode shapes of conductors at various loading stages. A turbulence signal is extracted from a set of full-scale data. It is added to the mean component of the downburst wind field previously evaluated from a CFD analysis. Dynamic analysis is performed using various downburst configurations. The study reveals that the response is affected by the background component, while the resonant component turns to be negligible due large aerodynamic damping of the conductors.

Keywords: dynamic analysis; free vibration; downburst; turbulence; finite element; transmission line conductors.

1. Introduction

Electricity is one of the most essential resources for the modern world. Because of this dependence, it is important to prevent the disruptions in the distribution of power, as disruptions can have severe social and economical consequences. Electricity is transmitted through conductors, supported by transmission towers. A major cause of power outages is the failure of the towers during severe natural disasters. These failures, causing losses of millions of dollars, have been often attributed to high localized wind events, in the form of tornadoes and downbursts (Manitoba Hydro 1999). Despite this fact, the design codes of transmission towers have typically considered only wind loads associated with large-scale synoptic events, such as hurricanes and typhoons. The resulting downburst velocity profiles are quintessentially different from these boundary layer wind profiles and can, therefore, produce completely different loading and collapse modes, as shown by Kim *et al.* (2007) for the case of tall buildings.

A downburst is defined as a strong downdraft that induces an outburst of damaging winds on, or

* Corresponding Author, Assistant Professor, E-mail: damatty@uwo.ca

near the ground (Fujita 1990). "A short-duration localized wind event results during a downburst, when the downdraft forms ring vortices and spreads radially as it strikes the ground, producing high horizontal wind velocities." The localized nature of the event (both spatially and in time) and the associated vortex dominated flow complexity are the biggest challenges in performing structural analysis, since the intensity of the wind velocity varies significantly with the characteristics of the downburst. The jet diameter (D_j), the location of the downburst center relative to the tower (represented by the polar coordinates r and θ) and the jet velocity (V_j) are the downburst characteristics, which significantly influence the distribution and magnitude of the forces acting on the tower and the conductors, as described by Shehata and El Damatty (2007) and Shehata *et al.* (2008).

Hangan and Kim (2004, 2007) developed and validated the computational fluid dynamic (CFD) model shown in Fig. 1 simulating the spatial and time variations of the wind field associated with downbursts. This fluid dynamic model simulates the large scale fluctuating mean component of the downburst velocity field.

Wang *et al.* (2009) studied the wind-induced dynamic response of high-rise transmission towers under downburst wind load. Wind tunnel tests were used to obtain the wind load coefficients of the transmission towers. The time history of the moving downburst horizontal fluctuating wind velocity was generated numerically considering the wind azimuth's continuous change. The transmission tower was dynamically analyzed under downburst loading. The analysis showed that the downburst size had the major effect on the displacement response of the transmission tower, while its dynamic effect on the tower was minor.

Mason *et al.* (2009) performed a numerical simulation in which the wind field of a microburst was studied. The simulated downburst had a primary and counter rotating secondary ring vortex at the leading edge of the diverging front. The development and structure of the outflow were significantly affected by the counter-rotating vortex. It was found that for loading isolated structures, the kinetic energy available within each simulated storm event was less than the energy available within atmospheric boundary layer winds.

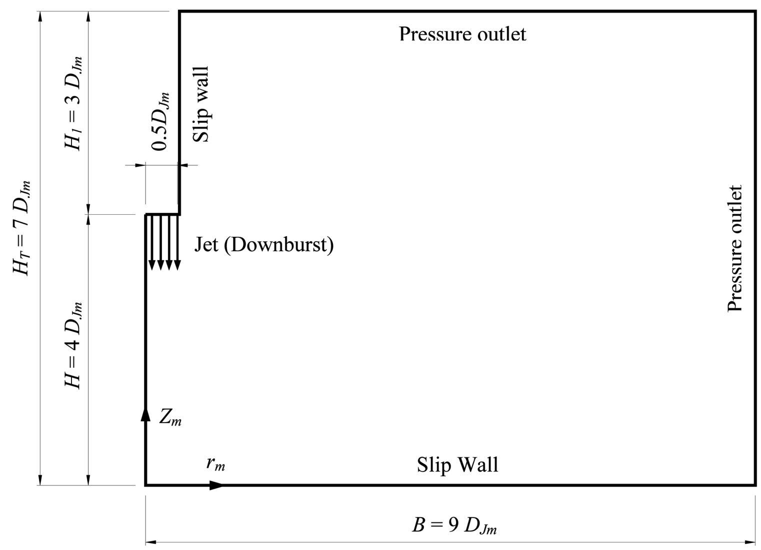

Fig. 1 Schematic diagram of computational domain of downburst CFD model (Hangan *et al.* 2003)

Kwon and Kareem (2009) presented a new analysis framework, which is called the gust-front factor approach, to design buildings subjected to gust-front winds (as downbursts). This is similar to the gust loading factor format used in codes and standards worldwide for conventional boundary layer winds. The developed factor is proposed to be used to scale-up the conventional wind loads so as to match the loads resulting from gust-front winds. This approach includes the effects of various factors affecting the loading due to gust-front winds. This factor is the product of four factors representing the variation in the vertical profile of wind speed (kinematic effects factor), dynamic effects introduced by the sudden rise in wind speed (pulse dynamics factor), nonstationarity of turbulence in gust-front winds (structural dynamics factor), and transient aerodynamics (potential load modification factor).

Shehata *et al.* (2005) developed a structural analysis numerical model for the evaluation of the response of transmission lines under the effect of downbursts. The CFD data developed by Hangan and Kim (2004) was incorporated in this model and was scaled-up based on the relative values between the characteristics of a prototype downburst and those used in the CFD model. Shehata *et al.* (2005) structure analysis model is based on the finite element method, and uses three-dimensional linear frame elements to simulate the tower members and two-dimensional non-linear curved frame elements to simulate the conductors.

Using this structure analysis model, Shehata and El Damatty (2007) conducted a parametric study by varying the jet diameter (D_j) and the location of the downburst center relative to the tower. A guyed transmission tower located in Manitoba, Canada, which collapsed in 1996 due to a downburst event, was used to perform this parametric study. The critical downburst parameters (D_j, r and θ), leading to maximum forces in the tower members, are identified. The study revealed that the critical downburst parameters vary based on the type and location of the members. For example, the chord members of the tower main body, the diagonal members of the tower main body, and the cross arms members are all found to have different critical downburst parameters. Shehata and El Damatty (2008) extended their numerical scheme by including a failure model for the tower member, which was used to study the progressive collapse of the guyed tower that failed in Manitoba, Canada in 1996. In lieu of the extensive parametric study, Shehata *et al.* (2008) extended the structural analysis model by including an optimization routine. This model is capable of predicting the critical downburst parameters and the corresponding forces in an automated procedure.

All the above studies were conducted in a quasi-static manner using the large scale fluctuating mean components of the downburst wind field, as predicted numerically by Hangan and Kim (2004, 2007). The use of a quasi-static analysis was justified based on the fact that the period of the large scale fluctuating mean component of the downburst load is significantly larger than the fundamental periods of oscillation of both the conductors and the tower. The inclusion of the turbulent component in the analysis can magnify the response due to combined effects of the fluctuating (background) component and the resonant component. The assessment of the effect of turbulence necessitates the incorporation of a turbulence model for the downburst wind field and also requires conducting a dynamic analysis. It is expected that the dynamic effect will be of more importance in analyzing the conductors rather than the tower as the conductors have typically larger fundamental periods compared to the tower and, consequently, are closer to the dominant periods of the turbulent component. The focus of the current study is the assessment of the effect of turbulence on the response of the conductors to downbursts.

Barbieri *et al*. (2004a, b). studied the dynamic behavior of transmission line conductors numerically using the finite element method and verified their results experimentally with three different sample lengths using five accelerometers placed along half the sample. The modal parameters were optimized through a gradient search routine, the complex envelope, and the single degree-of-freedom method. A reduced damping matrix was fitted by considering the first five free vibration modes. The study was extended to identify the structural damping of the conductors, which is found to be negligible in comparison to the aerodynamic damping. Barbieri *et al.* (2008) extended their previous studies to include the nonlinear characteristics of the transmission line conductors, presenting the results for simply supported inclined conductors. Experimental data obtained in an automated testing system for the conductors were used to validate the results.

Gattulli *et al.* (2007) assessed the ability of various numerical techniques to accurately reproduce the dynamic response of a suspended cable subjected to an artificially generated 3D turbulent wind field. Due to the high level of aerodynamic damping, weak nonlinear modal coupling was found in the dynamic responses of the studied cable. The high level of aerodynamic damping was also discussed by Loredo-Souza and Davenport (1998) in their study conducted to assess the dynamic behavior of transmission lines under severe normal wind loading. This study was performed experimentally, and the results were verified statistically. The effect of scale turbulence was studied, and the response of the structure was found to depend strongly on the turbulence intensity. In this study, it was concluded that the background response is the largest contributor to the total fluctuating response, in most typical cases. The resonant component can hold importance only when cable characteristics and flow conditions dictate a smaller value for the aerodynamic damping.

Chay *et al.* (2008) studied the variation of the peak gust intensity in non-stationary winds of different durations. A typical downburst was simulated repeatedly using a numerical model of downburst non-turbulent winds, and an amplitude-controlled Gaussian stochastic process for the turbulent component. The peak gust strength of each event was expressed as a peak factor (ratio) in relation to the largest non-turbulent speed. It was found the peak factor increases when the downburst event duration increases and it also increases when the turbulence intensity increases.

In order to assess the dynamic response of transmission line conductors under downburst loading, the dynamic characteristics of the conductors, including their natural frequencies and mode shapes, have to be determined. In addition, a turbulence model for downbursts has to be identified. Accordingly, the research presented in this paper is divided into three parts. In the first part of the study, the numerical model for the conductors adopted by Shehata *et al.* (2005), is extended to include dynamic analysis, as well as free vibration analysis for identification of the natural frequencies and mode shapes. Due to the high flexibility of the conductors, their natural frequencies can be affected by the pre-tensioning axial forces, the sagging and the stresses resulting from the downburst loading. As such, the free vibration analysis is conducted at each time increment, using an updated stiffness matrix that incorporates all of these effects. Full scale data obtained from field measurements of the velocity wind field during a downburst event are presented in the second part of the study. The turbulent component of this set of data is extracted, and used as the basis of the turbulence model for downburst simulation. Using the numerical model developed in the first part and the turbulence model proposed in the second part, along with the large scale fluctuating mean component of the downburst wind field obtained from the CFD model, a set of dynamic analyses are conducted to assess the effects of turbulence and dynamic behavior on the response of the conductors to downbursts.

A brief description of the finite element model, along with the extension of the model to include dynamic and free vibration analysis of non-linear flexible systems, is first provided. The three parts of the study described above are then presented followed by a discussion for the main conclusions obtained from the study.

2. Numerical modelling of the conductors

2.1 Finite element model for the conductors

The numerical model is based on a two dimensional consistent curved frame element that was developed by Koziey and Mirza (1994), and then extended to include the geometric non-linear effect by Gerges and El Damatty (2002). A sketch of a typical consistent curved frame element is shown in Fig. 2. The element formulation is based on C_o continuity – which is providing inter-element continuity of all degrees of freedom without providing this continuity for the first derivatives of the degrees of freedom – as interpolations of displacements (u and w) and through thickness rotations (α and φ) are conducted independently; interpolations of displacements are achieved using cubic polynomials considering the degrees of freedom at nodes 1, 2, 4 and 5, while the rotations are interpolated using quadratic polynomials considering the degrees of freedom at nodes 1, 3 and 5. In the nonlinear model of the consistent frame element, the solution is carried out incrementally while iterations are conducted within each increment until convergence is achieved. In the current study, the nonlinear model is extended by including an eigen-value routine within each increment. As such, the natural frequencies and mode shapes of the modeled structure are evaluated at each increment. Hence, the model can predict the variations of the dynamic characteristics of a conductor due to the large deformations expected from severe wind loading. The nonlinear model is also capable of accounting for the effects of the conductors' pre-tension force and initial sagging in estimating the stiffness of the conductors. More details about this finite element model are explained by Shehata *et al.* (2005).

2.2 Physical and geometric properties of the conductor

A six-span conductor, having the same properties (shown in Table 1) as the conductor modeled by Shehata *et al.* (2005), was considered. Each span has a length of 480 m, sag of 20 m, and is divided into five equal elements. The conductor is initially pre-tensioned with a force of 82,344 N. At the conductor-towers connections, a set of nonlinear springs, simulating the combined stiffness of the

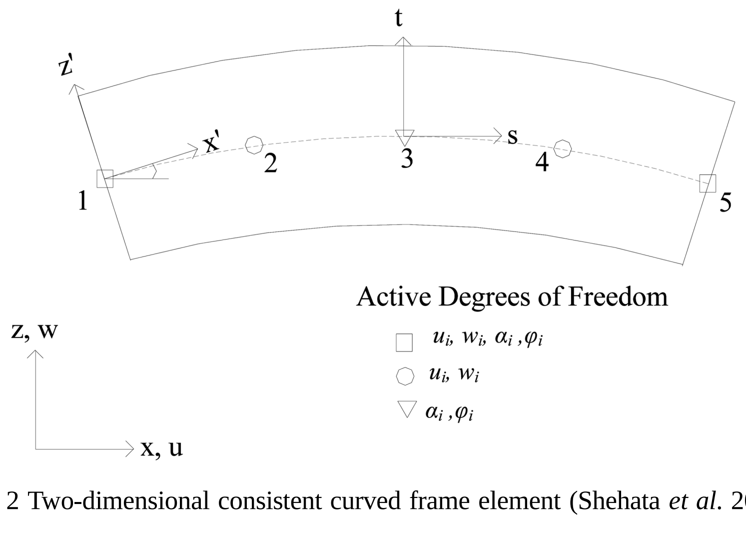

Fig. 2 Two-dimensional consistent curved frame element (Shehata *et al.* 2005)

Table 1 Physical parameters employed for conductor (Oakes 1971)

Parameter	Conductor
Name	1843.2 MCM 72/7 NELSON ACSR
Wind Span (m)	480
Diameter (mm)	40.64
Weight (N/m)	28.97
Modulus of elasticity (N/m^2)	6.23E10
Sag (m)	20.00

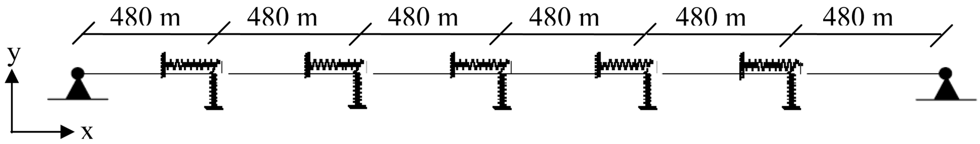

Fig. 3 Modeling of the transmission line under study

tower and the insulators, is implemented in the model as shown in Fig. 3. More details about the modeling of the conductors, including the evaluation of the springs' characteristics, are explained by Shehata *et al.* (2005).

2.3 Validation

The commercial program SAP2000 (Computers and Structures 2006) is used to validate the free vibration scheme incorporated into the numerical model. It is not possible to account for the effect nonlinear springs in a free vibration analysis conducted using SAP2000. Accordingly, for validation purpose, the analysis is conducted using SAP2000, while assuming hinge boundary conditions instead of the springs. An initial pre-tensioning force of 82,344 N is applied in the analysis with initial sag of 20 m. The results of the conducted analysis are summarized in Table 2 and Fig. 4, showing an excellent agreement, for both the mode shapes and the natural periods, between the model and the SAP2000 results.

3. Incremental free vibration analysis of the conductor

3.1 Incremental free vibration analysis of the conductor under uniform loading

As mentioned above, the free vibration analysis is conducted at various time increments accounting for the deformations under the applied wind load. The first set of free vibration analyses considers uniformly distributed forces associated with normal wind loads. The velocity of the assumed wind load is increased incrementally from zero to a value of 35 m/s, within ten increments. The results of the free vibration analysis conducted at the ten load increments have shown no differences in terms of natural frequencies and mode shapes of the structure. The values of the first four natural periods are shown in Table 2, and the mode shapes of the first three modes are plotted in Fig. 5. This result indicates that the magnitude of loading has no effect on the dynamic characteristics of the conductors.

Table 2 Results of the Eigen-value Analysis of the 6 Spanned Conductor

				T_1 (s)	T_2 (s)	T_3 (s)	T_4 (s)	T_5 (s)
Validation		MODEL		8.04	8.01	7.94	7.83	7.75
		SAP		8.02	8.03	7.95	7.84	7.76
		% Difference		0.34%	-0.32%	-0.18%	-0.03%	-0.02%
Uniform Load				12.20	11.30	10.19	9.15	8.33
Pre-tensioning Force Variation		400%		10.00	8.14	6.52	5.33	4.21
		200%		10.93	9.61	8.19	7.00	5.98
		100%		12.20	11.30	10.19	9.15	8.33
		50%		14.27	13.68	12.91	12.15	11.45
Boundary Condition Variation		Springs		12.20	11.30	10.19	9.15	8.33
		Hinged		8.04	8.01	7.94	7.83	7.75
Downburst Loading Case	D_J (m)	r/D_J	θ^o					
1	1000	1.6	30	12.00	11.11	10.03	8.99	7.87
2	1000	1.2	0	12.15	11.28	10.17	9.13	8.01
3	500	1.2	90	12.20	11.30	10.19	9.15	8.36

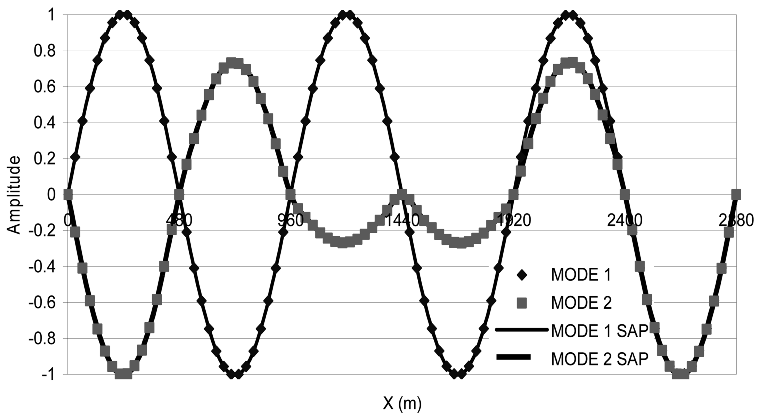

Fig. 4 Comparisons between mode shapes predicted by model and SAP 2000

3.2 Variation of the pre-tensioning level of the cables

The analysis under uniform loading is repeated by varying the magnitude of the pre-tension force. Various values representing 50%, 200% and 400% of the initial pre-tensioning force are considered, respectively. The sag is inversely proportional to the pre-tension force. Accordingly, the sag values are divided by the same factor used to magnify the pre-tensioning force, e.g., when the pre-tensioning is doubled, the sag is halved.

The natural periods and the mode shapes resulting from this set of analyses are given in Table 2 and Figs. 6(a) and (b). The results show that the variation in the level of pre-tensioning causes some variation in the values of the natural periods. Typically, the periods decrease with the increase of the

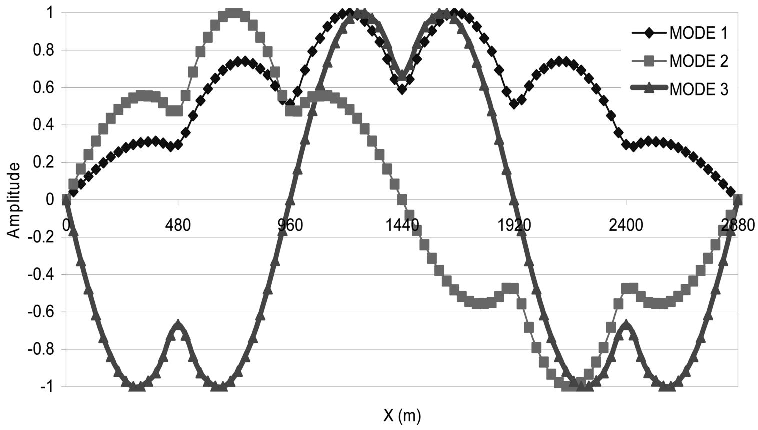

Fig. 5 First three mode shapes of the conductor under uniform load

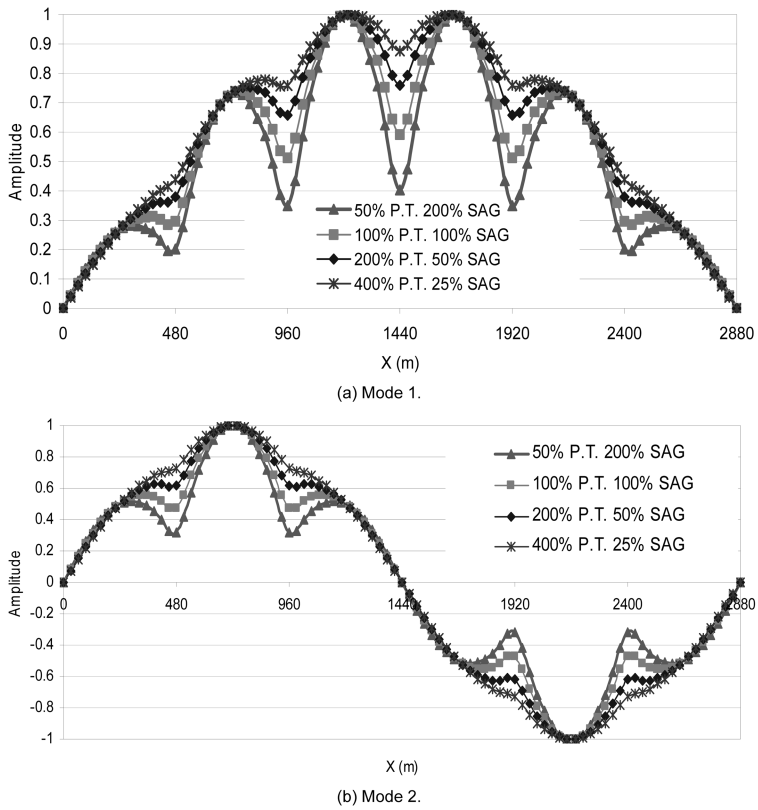

Fig. 6 Mode shapes of the conductor for different levels of pre-tensioning

pre- tensioning force. The differences between the periods of the first four modes are reduced with the reduction in the pre- tensioning force. It is also worth noticing the reduction of the mode shape amplitude at the spring locations when the magnitude of the pre- tensioning force is reduced. The reduction in the pre-tensioning force makes the effect of the intermediate conductor supports more significant. By comparing the results given in Table 2, it can be concluded that pre-tensioning force has a significant effect in increasing the stiffness of the conductor and consequently, decreasing its period of vibration.

3.3 Effect of the boundary conditions

In this section, the effect of the stiffness values at the connection between the towers and the conductors on the dynamic characteristics of the conductors is assessed. This is done by comparing the values obtained when intermediate springs are assumed to those obtained assuming intermediate hinges, as shown in Table 2. It can be noted that the periods associated with the spring case are well separated in comparison to the hinge case.

3.4 Analysis of the conductor under downburst loading

The dynamic characteristics of the conductor are then evaluated at different loading stages within a downburst event. The evaluation of the downburst forces followed the approach described by Shehata and El Damatty (2005). The downburst forces acting on the conductor depends on the parameters V_j, D_j, r/D_j and θ where V_j is the jet velocity, D_j is the jet diameter, r/D_j is the ratio between the distance between the centers of the downburst and the jet diameter and θ is the projection angle relative to the transverse direction of the transmission line. Three different downburst cases with parameters given in Table 2 are considered. They represent the most critical three different downburst configurations with respect to the considered transmission line, as predicted by Shehata and El Damatty (2005). The original pre-tensioning force, defined in section 3.1, is considered in all analyses. Free vibration analyses are conducted at the 240 time history load increments defining the entire time history of the loading (Shehata *et al.* 2005). The results of the analyses of the three load cases are given in Table 2. The results indicate almost no variation in the dynamic characteristics of the conductors within various time increments. The mode shapes shown in Fig. 7 are similar to those under uniform loading, with the exception of a minor loss of symmetry of the mode shapes. This is

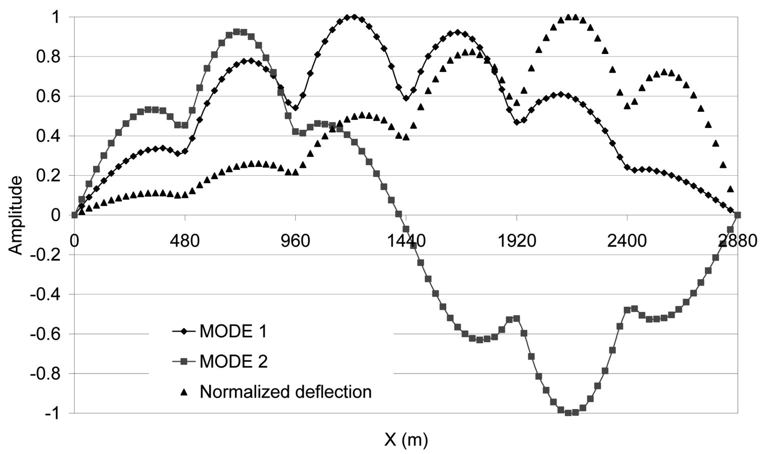

Fig. 7 First two mode shapes together with the normalized deflected shape of the conductor under load case #1

due to the asymmetric distribution of the downburst loading associated with this case.

In Fig. 7, the maximum deflection obtained through the time history analysis is normalized, such that the largest amplitude has a value of unity. It could be noted from the figure that the asymmetry of the deflected shape is more pronounced than the asymmetry of the mode shape.

4. Full scale data and turbulence extraction

4.1 Full scale data

The Wind Science and Engineering Research Centre at Texas Tech University recorded the gust front from a downdraft that occurred on the 4th of June 2002 at the former Reese Air force base, located 20 Km West of Lubbock, Texas, USA. The anemometers were placed at a 10 m height on four towers with a spacing of 263 m. The line of anemometer towers was in the North – South direction. The maximum recorded wind gust was approximately 40 m/s (which happened to be the 50-year return-period wind speed for this area, according to the ASCE-7). The fourth tower had additional anemometers at 2, 4, 6 and 15 m heights. Extensive details of these records are provided by Gast (2003) and Orwig and Schroeder (2007).

The set of data of the fourth tower was fitted, by Kim *et al*. (2007), with a set of CFD data corresponding to a downburst with a jet velocity of 29 m/s, and a diameter of 600 m. The data were used by Holmes *et al.* (2008) to isolate the turbulent component of the velocity and to produce a peak load reduction factor for the spatial variation along the longitudinal direction. This span reduction factor ranged between 1 and 0.8 within a distance of 720 m, which means that the maximum difference between the peak loads at any two points along the longitudinal direction is 20%. Hence the variation of turbulence along the longitudinal direction is considered to be negligible. In the same study, the vertical velocity profiles of the maximum running mean and the gust speeds are found to have negligible variation along the height of tower 4 (from 0 to 15 m). Therefore, the variation in turbulence along the height of the transmission tower (44 m) could be also considered negligible.

4.2 Turbulence extraction

The turbulence is extracted by calculating the moving average of the velocity over a certain period of time, and subtracting it from the total (instantaneous) velocity within this period of time. The averaging period (called the filtering or running mean period) could be as low as 10 s or as high as 120 s, as that used by Gast (2003) and Orwig and Schroeder (2007). In Fig. 8, the turbulence (light line) has been calculated by subtracting the running average velocity (the black solid line) from the full scale data (shown as dark dots). Holmes *et al.* (2008) calculated the running turbulence intensity (which is the ratio between the time-varying root mean squared turbulence and the running mean wind speed) for various filtering periods. The study showed that for averaging periods between 20 s and 80 s, the running turbulence intensity is stable between 0.09 and 0.12. Hence averaging periods within this range are considered to be suitable. According to Holmes *et al.* (2008), the use of averaging times higher than 80 s can incorrectly include part of the mean component of the velocity that should not be considered as random turbulence. On the other hand, averaging times lower than 20 s exclude a large portion of the random component from the residual

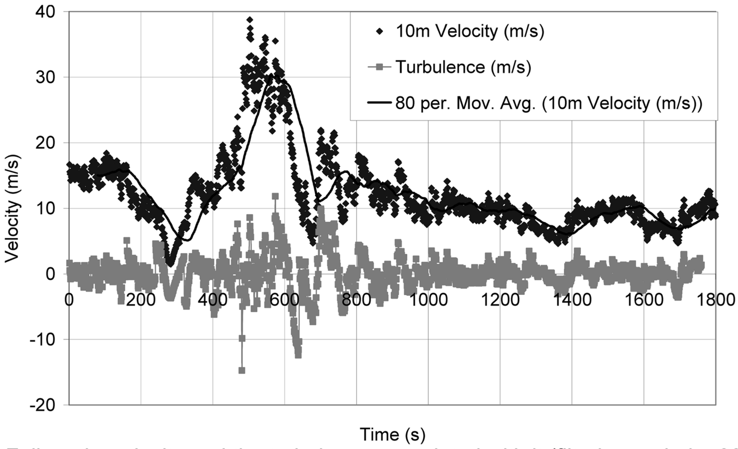

(a) Full scale velocity and the turbulence associated with it (filtering period = 80s).

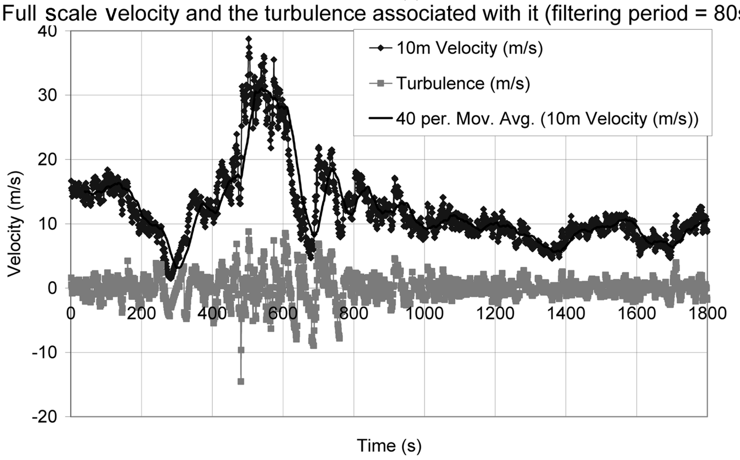

(b) Full scale velocity and the turbulence associated with it (filtering period = 40s).

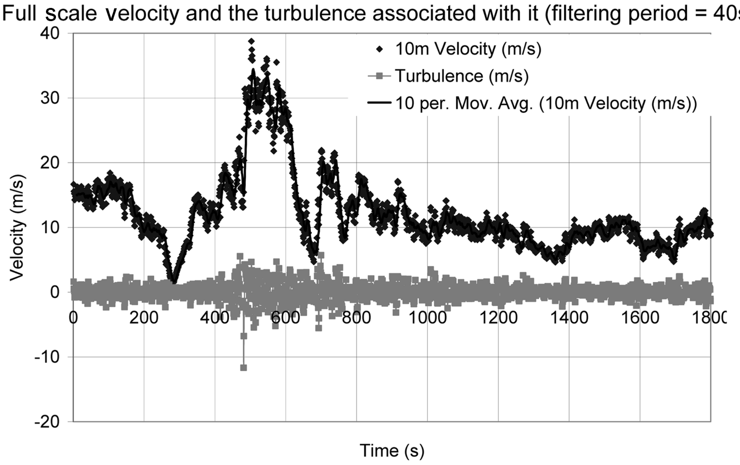

(c) Full scale velocity and the turbulence associated with it (filtering period = 10s).

Fig. 8 Full scale velocity at a height of 10 m and the turbulence associated with it

turbulence as stated by Holmes *et al.* (2008). The power spectrum of the full scale velocity shown in Fig. 9 is produced by transferring the full scale velocity data from the time domain to the

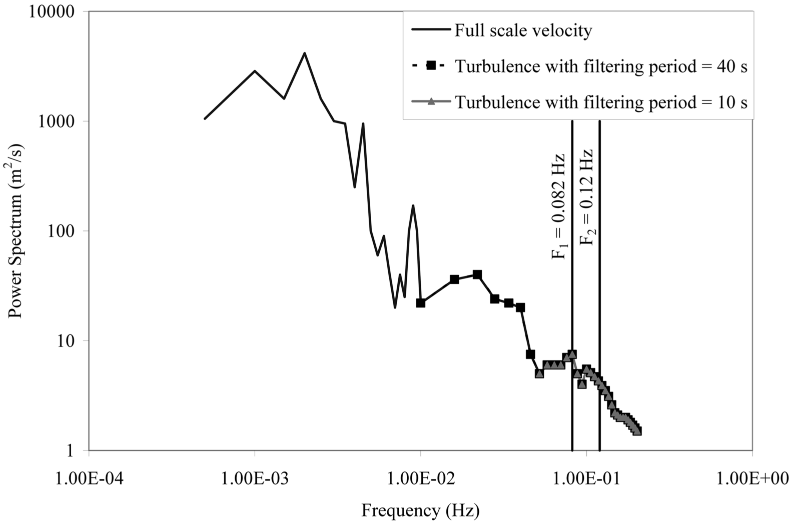

Fig. 9 Power spectra of the measured velocities

frequency domain through performing a Fourier transformation. The peaks occurring at frequencies less than 0.01 Hz represent the large scale (mean) component of the wind velocity. The range of natural frequencies of the conductor are identified in the figure by showing the fundamental frequency of the conductor F1 = 0.082 Hz and the frequency of the fifth mode F5 = 0.12 Hz. The large gap between the dominant frequencies of the mean component and the frequencies of the conductor can be shown in the figure. The power spectra for the filtered turbulent component for filtering periods of 10 s and 40 s are also provided in Fig. 9. The figure shows that the turbulent component occurs over a range of frequencies that are relatively close to the fundamental frequency of the conductor.

5. Dynamic analysis

The numerical model described previously in section 2 is used, together with the Newmark direct integration method, to perform nonlinear dynamic analyses. More details about the Newmark method are explained by Bathe (1996).

5.1 Validation

5.1.1 Sweep test

The first validation is done by conducting a sweep test, where the transmission line analyzed previously in section 3.1 is subjected to a uniform load that has a sinusoidal variation with time. The sweep test is conducted by varying the frequency of the applied load and recording the maximum mid-span deflection corresponding to each frequency value. The results of the sweep test show that the absolute maximum deflection occurs at an oscillating period of 12.2 s, which is very close to the fundamental period of the structure reported in section 3.1.

5.1.2 Time-History analysis for a simply supported shallow arch

A time history nonlinear analysis of a simply supported shallow arch previously modeled by Bathe *et al.* (1975), is conducted. The arch has a square cross-section of 0.0252 m. Other geometric and material properties of the arch are shown in Fig. 10(a). The arch is subjected to a uniformly distributed pressure of 3.83 MPa. The time history variation of the load is shown in Fig. 9(b). The time step used in the analysis is 3.315E-05s, which is equivalent to the fundamental period of the structure divided by 70. No damping is included in the dynamic analysis. The time history variation of the mid-span deflection resulting from the analysis is shown in Fig. 10(b), along with the results obtained by Bathe *et al.* (1975), showing an excellent agreement.

5.2 Damping

The structural damping of the cables is neglected in this study, since it is quite small relative to the aerodynamic damping. The aerodynamic damping (ζ_{ai}) for uniformly loaded cables for mode (i)

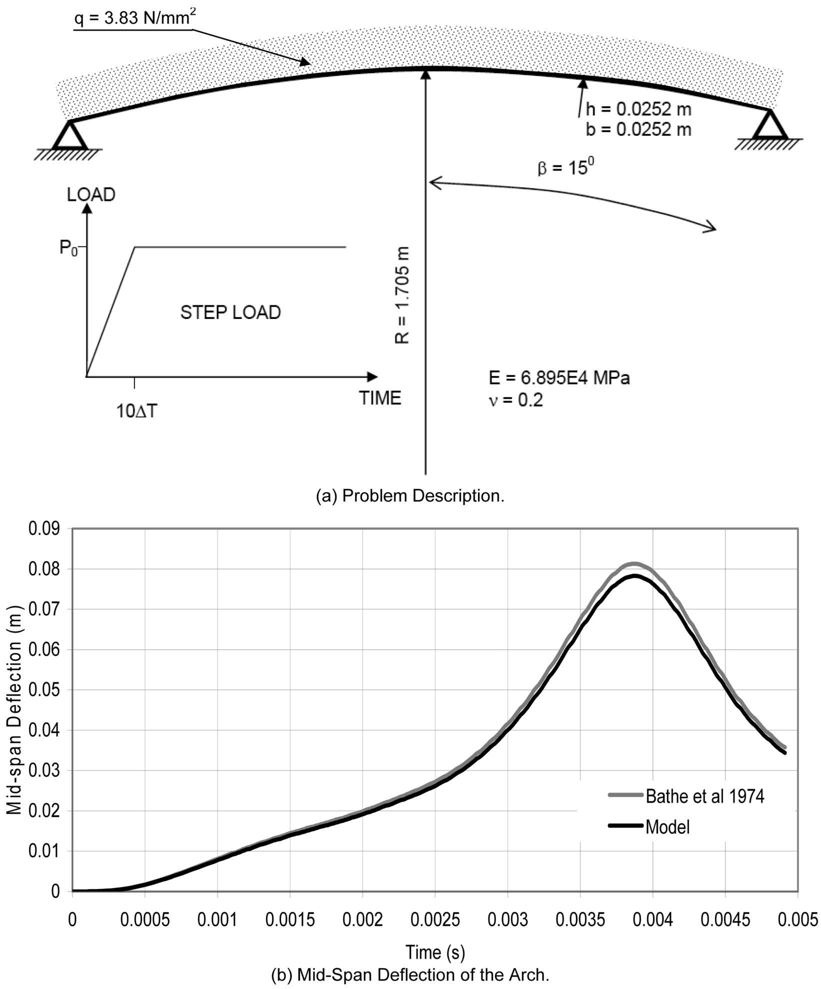

Fig. 10 Analysis of simply supported shallow arch under time-dependent loading

is computed using Eq. (1) that was originally developed by Davenport (1962), and adjusted by Macdonald (2002) to include the directional variation of the velocity.

$$(\zeta_a)_i = \frac{\rho C_D D_c V}{4\pi m_c f_i}(1 + \cos^2\phi) \tag{1}$$

Where ρ is the fluid density, D_c the cable diameter, m_c the mass of the cable per unit length, C_D the drag coefficient, and V and ϕ are the magnitude and direction of the wind velocity in the plane normal to the cable axis. Substituting the cable properties into the previous equation leads to values of aerodynamic damping of 17% and 34% for uniform wind velocities (normal to the cable) of 10 m/s and 20 m/s, respectively. Due to the localized nature of downbursts, the wind velocity varies with time and also spatially along the length of the conductor. To account for the effect of such a variation on the aerodynamic damping, an average wind velocity $V_{avg}(t)$ is calculated at each time step, as follows

$$V_{avg}(t) = \frac{1}{L}\int_0^L V(x)dx \tag{2}$$

Accordingly, the aerodynamic damping will vary with time depending on the time history variation of $V_{avg}(t)$. At each time step, the corresponding value of $V_{avg}(t)$ is substituted into Eq. (1) (replacing V) to obtain the instantaneous value of ζ_a

$$(\zeta_a)_i = \frac{\rho C_D D_c V}{4\pi m_c f_i}(1 + \cos^2 0) = \frac{2\rho C_D D_c V_{avg}}{4\pi m_c f_i} = \frac{\rho C_D D_c V_{avg}}{2\pi m_c f_i} \tag{3}$$

5.3 Analysis and results

Two types of time history loads are considered in the conducted analyses:

a) The large scale, running mean component of the downburst loading associated with the downburst configuration at which the failure has been initiated as described by Shehata and El Damatty (2007), which was: D_j = 1000 m, r/D_j = 1.6 and $\theta = 30^0$. The jet velocity has a value of 29 m/s, the same as that of the CFD-matched full-scale data, by Hangan and Kim (2007). The entire large scale wind velocity field is obtained from the CFD data. The forces corresponding to this component vary with time and space. As such, the time history of the forces acting at the tower and the conductors vary from one point to another, depending on the location of the specific point relative to the center of the downburst.
b) The turbulent component is obtained from the filed measurements. As explained before, based on the field measurements at various vertical locations, and based on the relatively high longitudinal correlations (Holmes *et al.* 2008), the turbulent component is assumed not to vary spatially. The time variation of this turbulent component depends on the employed filtering scheme.

The following set of time history analyses are conducted in this study:

· Analysis 1; Non-turbulent quasi-static analysis:

Includes the running mean component without adding the turbulent component. The analysis is conducted in a quasi-static manner, i.e., without considering the dynamic effect.

· Analysis 2; Turbulent quasi-static analysis:
Includes the running mean and the turbulent components. This analysis is repeated several times, using different values for the filtering period. The filtering periods used are 10 s, 20 s, 30 s, 40 s and 80 s, respectively. The analysis is conducted in a quasi-static manner, i.e., without considering the dynamic effect.

· Analysis 3; Non-turbulent undamped dynamic analysis:
Includes the running mean component without adding the turbulent component. The dynamic effect is included and zero damping is assumed (undamped).

· Analysis 4; Turbulent undamped dynamic analysis:
Includes the running mean and the turbulent components. This analysis is repeated several times, using different values for the filtering period. The used filtering periods are 10 s, 20 s, 30 s, 40 s and 80 s, respectively. The dynamic effect is included and zero damping is assumed (undamped).

· Analysis 5; Turbulent 17% damped dynamic analysis:
Includes the running mean and the turbulent components. This analysis is repeated several times, using different values for the filtering period. The filtering periods used are 10 s, 20 s, 30 s, 40 s and 80 s, respectively. The dynamic effect is included. A constant aerodynamic damping of 17% (corresponding to a uniform wind velocity of 10 m/s) is assumed.

· Analysis 6; Turbulent 34% damped dynamic analysis:
Includes the running mean and the turbulent components. This analysis is repeated several times, using different values for the filtering period. The filtering periods used are 10 s, 20 s, 30 s, 40 s and 80 s, respectively. The dynamic effect is included. A constant aerodynamic damping of 34% (corresponding to a uniform wind velocity of 20 m/s) is assumed.

· Analysis 7; Turbulent dynamic analysis with variable damping:
Includes the running mean and the turbulent components. This analysis is repeated several times, using different values for the filtering period. The filtering periods used are 10 s, 20 s, 30 s, 40 s and 80 s, respectively. The dynamic effect is included. The time varying aerodynamic damping explained in section 5.2, is included in this analysis.

The spatial variations of the maximum transverse deflections, obtained from the above set of time history analyses are plotted in Figs. 11 and 12(a), (b) and (c). Fig. 11 illustrates a comparison between the results obtained from analyses 1 to 7 for a filtering time of 30s, while Figs. 12(a), (b) and (c) show the results corresponding to the filtering times of 10s, 40s and 80s, respectively.

When observing the results in Figs. 11 and 12(a), (b) and (c), one can notice the following:

· The quasi-static analysis of the non-turbulent wind loaded line results in the smallest deflections, while the undamped dynamic analysis of the turbulent wind loaded line gives the largest deflections.

· Due to the fact that the frequencies of the mean component are much lower than the natural frequencies of the structure, the undamped dynamic analysis of the non-turbulent wind loaded line produces a deflection very near to that of the quasi-static analysis of the non-turbulent wind loaded line.

· As the filtering period decreases, the response due to turbulence decreases. This is due to the exclusion of a portion of the random component from the residual turbulence when decreasing the filtering period.

· The increase in the responses due to turbulence increases with the increase in the filtering periods until 40 s, after which the rate of increase decreases, suggesting that 40 s would be a suitable averaging period.

· Due to the high aerodynamic damping, the damped dynamic analysis of the turbulent wind loaded line (with different values of damping ranging between 17% and 34%) produces a deflection

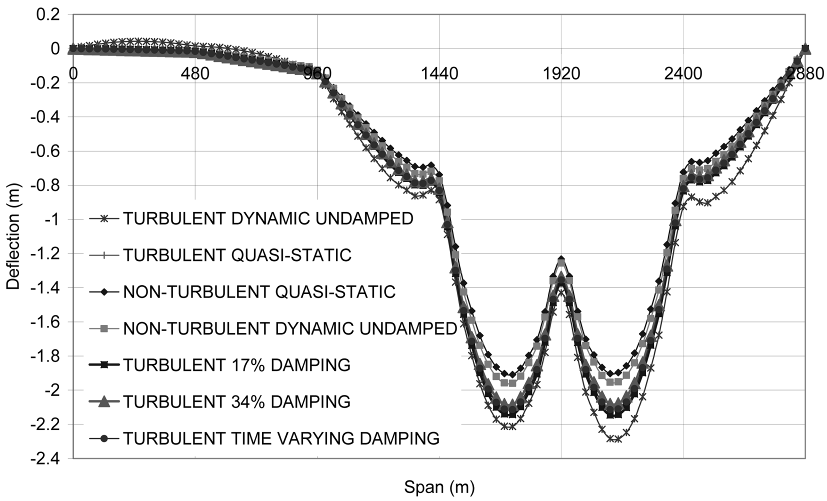

Fig. 11 Deflection with varying damping due to downburst with 30s filtering time

very near to that of the quasi-static analysis of the turbulent wind loaded line as the high aerodynamic damping significantly reduces the resonant response.

Some selected results obtained from the analyses are also provided in Table 3. The maximum transverse deflections, as well as the maximum transverse and longitudinal reactions at the intermediate spring, are provided in this table. These reactions represent the maximum forces transferred from the conductors to the intermediate tower. The maximum values corresponding to the quasi-static (QT), undamped non-turbulent dynamic (NT), and undamped turbulent dynamic (UT), are provided. The response of the conductor to turbulence consists of two components: the background component (B) and the resonant component (R). These components are isolated using the following relations:

$$B = QT - NT; \; R = UT - QT$$

The percentages of each of these two components relative to the undamped turbulent dynamic (UT) cases are provided in Table 3, for filtering times of 10 s, 20 s, 30 s, 40 s and 80 s, respectively. The following observations can be drawn from these results:

- The values of deflections shown in Table 3 show that for an undamped line with lower turbulence filtering periods, the resonant response is higher than the background response (for 10 s filtering period). For longer filtering periods (40 s and 80 s), the resonant response is lower than the background response.
- The reactions presented in Table 3 show that as the filtering period decreases, the values of the reactions of the undamped dynamic analysis of the turbulent wind loaded line approach those resulting from the quasi-static analysis of the turbulent wind loaded line. It could be also noticed that the ratio between the resonant and background components increases when the filtering period decreases.
- As the filtering period decreases, the background component of the turbulence decreases. This is due to the exclusion of a portion of the random component from the residual turbulence when decreasing the filtering period. This excluded portion has a range of frequencies that is significantly less than the natural frequencies of the conductor (as shown in Figs. 11 and 12(a), (b) and (c) and Table 3), causing a decrease in the background component in comparison to the resonant component.

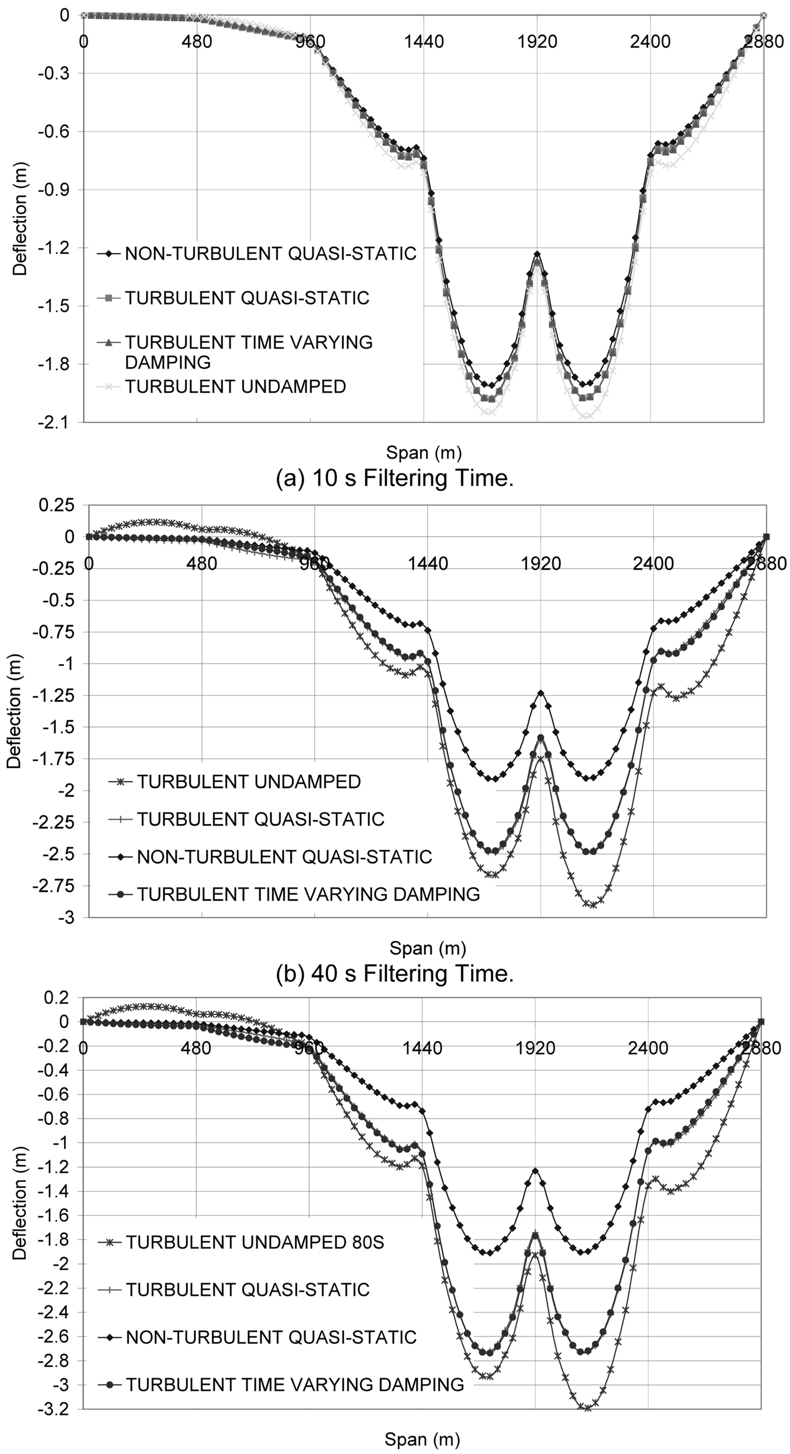

(a) 10 s Filtering Time.

(b) 40 s Filtering Time.

(c) 80 s Filtering Time.

Fig. 12 Deflection due to downburst for different filtering periods

Table 3 Effects of Turbulence on the Quasi-Static and Dynamic Responses of the Conductors

Transverse Deflection (m)					
FILTER TIME (s)	10	20	30	40	80
NT: Non turbulent	1.91	1.91	1.91	1.91	1.91
QT: Quasi-Static turbulent	1.97	2.05	2.14	2.48	2.73
UT: Undamped turbulent	2.07	2.19	2.33	2.90	3.19
B: Background Deflection = QT-NT	0.06	0.15	0.23	0.57	0.63
R: Resonant Deflection = UT-QT	0.10	0.13	0.19	0.42	0.46
% Background Component = 100*B/UT	3.1%	6.6%	10.0%	19.7%	19.9%
% Resonant Component = 100*R/UT	4.6%	6.2%	8.1%	14.5%	14.9%
R/B	1.51	0.93	0.81	0.73	0.73
Transverse Reaction (N)					
FILTER TIME (s)	10	20	30	40	80
NT: Non turbulent	-5720	-5720	-5720	-5720	-5720
QT: Quasi-Static turbulent	-6030	-6250	-6530	-7600	-8360
UT: Undamped turbulent	-6330	-6630	-6970	-8370	-9250
B: Background transverse reaction = QT-NT	-310	-530	-810	-1890	-2650
R: Resonant transverse reaction = UT-QT	-300	-380	-450	-760	-880
% Background Component = 100*B/UT	4.9%	8.0%	11.6%	22.6%	28.6%
% Resonant Component = 100*R/UT	4.8%	5.8%	6.4%	9.1%	9.5%
R/B	0.97	0.72	0.55	0.40	0.33
Longitudinal Reaction (N)					
FILTER TIME (s)	10	20	30	40	80
NT: Non turbulent	13780	13780	13780	13780	13780
QT: Quasi-Static turbulent	14530	15060	15730	18330	20160
UT: Undamped turbulent	15270	16000	16930	20230	22320
B: Background reaction = QT-NT	750	1280	1950	4550	6380
R: Resonant longitudinal reaction = UT-QT	740	940	1190	1900	2160
% Background Component = 100*B/UT	4.9%	8.0%	11.5%	22.5%	28.6%
% Resonant Component = 100*R/UT	4.8%	5.9%	7.1%	9.4%	9.7%
R/B	0.99	0.73	0.61	0.42	0.34

- The resonant component of the turbulence is damped out when the damping is included in the analysis, leaving the background component to play the major role in the quantification of the effect of turbulence. Consequently, the turbulent damped dynamic system produces results very near to those produced from the turbulent quasi-static system.
- Whereas the resonant component is damped out due to the high aerodynamic damping, the background component (B) represents the real increase in the reaction due to turbulence.
- The response due to turbulence significantly increases with the increase in the filtering periods, between filtering periods of 10 s and 40 s. Between filtering periods of 40 s and 80 s, the response remains almost unchanged. Hence, a filtering period of 40 s is considered to be sufficient enough

for quantifying turbulence, as also concluded by Holmes *et al.* (2008). Therefore, it could be concluded that the increase in the reactions due to turbulence is 22.5%, which corresponds to the percentage of background component for a filtering period of 40 s. On the other hand, the increase in the transverse deflection due to turbulence is 19.7%, which corresponds to the percentage of background component for a filtering period of 40 s.

6. Conclusions

The following conclusions can be drawn from this study:

1. The magnitude of the pre-tensioning forces has a major effect on the natural frequencies, reactions and mode shapes of the conductor. As the pre-tensioning force increases, the natural periods of the structure decreases, and the deflection at the connection between the towers and the cables increases, causing the structure to behave more as a cable than a beam.
2. The inclusion of the flexibility of the towers and insulators at the towers/conductor connections, rather than assuming fully hinged boundary conditions, has a significant effect on the natural frequencies and mode shapes.
3. Neither the level of loading nor the downburst load configuration has any significant effect on the natural periods and the mode shapes of the conductor.
4. The response due to turbulence increases significantly with the increase in the filtering periods, until a filtering period of 40 s. Beyond this value, the response remains almost unchanged. This suggests that 40 s is a suitable averaging period, agreeing with the findings of Holmes *et al.* (2008).
5. Due to the large aerodynamic damping, the resonant component of the turbulence is damped out when the damping is included in the analysis, leaving the background component to play the major role in the quantification of the effect of turbulence. Hence, the quasi-static analysis is sufficient enough in assessing the effect of turbulence.
6. Considering the 40 s averaging period, the inclusion of turbulence increases the deflection and the internal forces by about 20% for the considered downburst intensity.

Acknowledgements

The authors would like to acknowledge Manitoba Hydro, CEATI and the Natural Sciences and Engineering Research Council of Canada (NSERC) for their extensive financial support of this research project and Dr. Mohamed Moftah and Dr. Ahmed Shehata for their exclusive help in the production of this paper.

References

Bathe, K.J. (1996), *Finite Element Procedures in Engineering Analysis*, Prentice-Hall, Englewood Cliffs, New Jersey.

Bathe, K.J., Ramm, E. and Wilson, E.L. (1975), "Finite element formulations for large deformation dynamic analysis", *Int. J. Numer. Meth. Eng.*, **9**(2), 353-386.

Barbieri, N., de Souza, O.H. and Barbieri, R. (2004a), "Dynamical analysis of transmission line cables. Part 1 -

Linear theory", *Mech. Syst. Signal Pr.*, **18**(3), 659-669.

Barbieri, N., de Souza, O.H. and Barbieri, R. (2004b), "Dynamical analysis of transmission line cables. Part 2 - Damping estimation", *Mech. Syst. Signal Pr.*, **18**(3), 671-681.

Barbieri, N., de Souza, O.H. and Barbieri, R. (2008), "Dynamical analysis of transmission line cables. Part 3- Nonlinear theory", *Mech. Syst. Signal Pr.*, **22**(4), 992-1007.

Chay, M.T., Wilson, R. and Albermani, F. (2008), "Gust occurrence in simulated non-stationary winds", *J. Wind Eng. Ind. Aerod.*, **96**(10-11), 2161–2172.

Computers and structures (2006), SAP 2000 v11.01.

Davenport, A.G. (1962), "Buffeting of a suspension bridge by storm winds", *J. ASCE Struct. Div.*, **88** (3), 233-264.

Fujita, T.T. (1990), "Downbursts: meteorological features and wind field characteristics", *J. Wind Eng. Ind. Aerod.*, **36**(1), 75-86.

Gattulli, V., Martinelli, L., Perotti, F. and Vestroni, F. (2007), "Dynamics of suspended cables under turbulence loading: reduced models of wind field and mechanical system", *J. Wind Eng. Ind. Aerod.*, **95**(3), 183-207.

Gast, K.D. (2003), *A comparison of extreme wind events as sampled in the 2002 Thunderstorm Outflow Experiment*, Master's Thesis, Texas Tech University, Lubbock.

Gerges, R.R. and El Damatty, A.A. (2002), "Large displacement analysis of curved beams", *Proceedings of the CSCE Conference*, ST 100, Montreal, QC, Canada.

Hangan, H. and Kim, J. (2004), "Numerical simulation of downbursts", *Proceedings of the ASCE Structural Congress*, Nashville, Te, USA, June.

Hangan, H. and Kim, J. (2007), "Numerical simulations of impinging jets with application to downbursts", *J. Wind Eng. Ind. Aerod.*, **95**(4), 279–298.

Holmes, J.D., Hangan, H.M., Schroeder, J.L., Letchford, C.W. and Orwig, K.D. (2008), "A forensic study of the Lubbock-Reese downdraft of 2002", *Wind Struct.*, **11**(2), 137-152.

Kim, J., Hangan, H. and Ho, T.C.E. (2007), "Downburst versus boundary layer induced loads for tall buildings", *Wind Struct.*, **10**(5), 481-494.

Koziey, B.L. and Mirza, F.A. (1994), "Consistent curved beam element", *Comput. Struct.*, **51**(6), 643-654.

Kwon, D.K. and Kareem, A. (2009), "Gust-front factor: New framework for wind load effects on structures", *J. Struct. Eng.-ASCE*, **135**(6), 717-732.

Loredo-Souza, A.M. and Davenport, A.G. (1998), "The effects of high winds on transmission lines", *J. Wind Eng. Ind. Aerod.*, **74-76**, 987-994.

Macdonald, J.H.G. (2002), "Separation of the contributions of aerodynamic and structural damping in vibrations of inclined cables", *J. Wind Eng. Ind. Aerod.*, **90**(1), 19-39.

Mason, M.S., Wood, G.S. and Fletcher, D.F. (2009), "Numerical simulation of downburst winds", *J. Wind Eng. Ind. Aerod.*, **97**(11-12), 523–539.

Manitoba Hydro Transmission and Civil Design Department (1999), *Bipole 1 & 2 HVDC Transmission Line Wind Storm Failure on September 5, 1996 – Review of Emergency Response, Restoration and Design of These Lines*, Manitoba Hydro, 98-L1/1-37010-06000, 54.

Oakes, D. (1971), "Nelson river HVDC transmission line towers", *Proceedings of the Manitoba Power Conference EHV-DC*, Winnipeg, Manitoba, Canada, June.

Orwig, K.D. and Schroeder, J.L. (2007), "Near-surface wind characteristics of extreme thunderstorm outflows", *J. Wind Eng. Ind. Aerod.*, **95**(7), 565-584.

Shehata, A.Y., El Damatty, A.A. and Savory, E. (2005), "Finite element modelling of transmission line under downburst wind loading", *Finite Elem. Anal. Des.*, **42**(1), 71-89.

Shehata, A.Y. and El Damatty, A.A. (2007), "Behaviour of guyed transmission line structures under downburst wind loading", *Wind Struct.*, **10**(3), 249-268.

Shehata, A.Y. and El Damatty, A.A. (2008), "Failure analysis of a transmission tower during a microburst", *Wind Struct.*, **11**(3), 193-208.

Shehata, A.Y., Nassef, A.O. and El Damatty, A.A. (2008), "A coupled finite element-optimization technique to determine critical microburst parameters for transmission towers", *Finite Elem. Anal. Des.*, **45**(1), 1-12.

Wang, X., Lou, W., Li, H. and Chen, Y. (2009), "Wind-induced dynamic response of high-rise transmission tower under downburst wind load", *J. Zhejiang Univ.*, **43**(8), 1520-1525.

JH